Input-output analysis of high-speed axisymmetric isothermal jet noise

Jinah Jeun,[1,a)] Joseph W. Nichols,[1,b)] and Mihailo R. Jovanović[2,c)]
[1]*Department of Aerospace Engineering and Mechanics, University of Minnesota, Minneapolis, Minnesota 55455, USA*
[2]*Department of Electrical and Computer Engineering, University of Minnesota, Minneapolis, Minnesota 55455, USA*

(Received 23 September 2015; accepted 21 March 2016; published online 26 April 2016)

We use input-output analysis to predict and understand the aeroacoustics of high-speed isothermal turbulent jets. We consider axisymmetric linear perturbations about Reynolds-averaged Navier-Stokes solutions of ideally expanded turbulent jets with jet Mach numbers $0.6 < M_j < 1.8$. For each base flow, we compute the optimal harmonic forcing function and the corresponding linear response using singular value decomposition of the resolvent operator. In addition to the optimal mode, input-output analysis also yields sub-optimal modes associated with smaller singular values. For supersonic jets, the optimal response closely resembles a wavepacket in both the near-field and the far-field such as those obtained by the parabolized stability equations (PSE), and this mode dominates the response. For subsonic jets, however, the singular values indicate that the contributions of sub-optimal modes to noise generation are nearly equal to that of the optimal mode, explaining why the PSE do not fully capture the far-field sound in this case. Furthermore, high-fidelity large eddy simulation (LES) is used to assess the prevalence of sub-optimal modes in the unsteady data. By projecting LES source term data onto input modes and the LES acoustic far-field onto output modes, we demonstrate that sub-optimal modes of both types are physically relevant. *Published by AIP Publishing.* [http://dx.doi.org/10.1063/1.4946886]

I. INTRODUCTION

The rapid growth of the aviation industry, from the development of high-performance military aircraft to the increase of civil aircraft traffic, has raised awareness of aviation noise as an environmental pollutant. This has resulted in increasingly stringent noise regulations so that reduction of aviation noise has become an important design parameter.

Jet noise modeling was pioneered by Lighthill's acoustic analogy,[1] which was then extended and generalized by Curle,[2] Ffowcs Williams,[3] Lilley,[4] and Goldstein.[5] The acoustic analogy rearranges the full Navier-Stokes equations exactly so that a wave propagation operator appears on the left hand side. The remaining terms on the right hand side are interpreted as acoustic sources. While exact acoustic analogies are most useful in identifying compact acoustic sources. Non-compact effects can only be recovered by two-point two-time correlations between source terms in convolution with an adjoint Green's function of the wave propagation operator.[6,7]

As Mollo-Christensen[8,9] first suggested, instability wave theory can greatly simplify and model non-compact effects associated with high-speed jets. Such wavepackets have been observed in experimental data[10] as well as high fidelity simulations.[11] Given a base flow, instability wavepackets can be predicted using the parabolized stability equations (PSE),[12–16] the one-way Euler equations,[17]

a)Electronic mail: jeunx002@umn.edu
b)Electronic mail: jwn@umn.edu
c)Electronic mail: mihailo@umn.edu

and global mode analysis.[18] All of these techniques are much less computationally expensive than large eddy simulation (LES) or direct numerical simulation (DNS).

While PSE analysis successfully models sound generation driven by small disturbances in supersonic jets,[14,15] it fails to fully recover the far-field acoustics of subsonic jets.[16] Wavepackets computed by the PSE for subsonic jets severely underpredict the far-field acoustics. One possible explanation for the large discrepancy between prediction and experimental measurements in this case is that the assumption of a steady base flow is too restrictive. Indeed, such jets are subject to unsteadiness at frequencies much lower than the frequencies associated with noise-producing wavepackets. In this scenario, noise-producing wavepackets respond to a slowly varying base flow, periodically visiting states of enhanced acoustic radiative efficiency. Capturing the acoustically intermittent nature of these jittering wavepackets is found to explain a portion of the missing sound in the peak jet noise direction.[19,20] A fraction of the noise remains missing, however, particularly in the sideline direction (acoustic radiation perpendicular to the flow direction).

In a recent study, global mode analysis found that the jet may support additional coherent modes of acoustic radiation. Nichols and Lele[18] extracted two different types of global modes in a study of a cold supersonic jet. In addition to modes corresponding to downstream-propagating Kelvin-Helmholtz instability waves, the analysis also predicted upstream-propagating modes. These upstream-propagating modes were found to correspond to one of the three families of instability waves of supersonic jets as predicted by the linear stability analysis of locally parallel flow.[21] Because analysis of the PSE depends on downstream marching, upstream-propagating modes are inevitably missed. While global mode analysis characterizes the dynamics of systems dominated by unstable modes, the high-speed jets we consider are, in fact, globally stable. These jets do support spatial growth of disturbances leading to wavepackets, but are globally stable in the sense that these disturbances eventually convect downstream and decay. In this case, the flow is best thought of as an amplifier, which filters external disturbances and amplifies noise (as opposed to globally unstable systems, which may be thought of as self-sustained oscillators). In the globally stable case, individual global modes are not sufficient to characterize the flow dynamics. Instead, an optimal forcing approach[22–25] works better for amplifier-type dynamics. The leading eigenvalue and corresponding eigenvector of the resolvent operator give respectively the optimal gain and optimal forcing at a given frequency.[26]

In this paper, we apply input-output analysis[27,28] to assess whether it can successfully predict the aeroacoustics of high-speed isothermal turbulent jets. To understand the sound generation mechanism associated with turbulent jets, we examine the spatial structure of forcing functions that optimally convert near-field aerodynamic fluctuations into far-field acoustics for both subsonic and supersonic jets. We also consider sub-optimal modes resulting from input-output analysis and investigate their role in the generation of sound. In particular, we find that in certain cases sub-optimal modes contribute significantly to sound generation and thus may explain a portion of the missing sound associated with PSE analysis. We note also that input-output modes are useful as a basis for constructing reduced-order models.[29]

The remainder of this paper is organized as follows. Sec. II defines the flow configurations and governing equations. The numerical method is also briefly explained. Results of input-output analysis of subsonic and supersonic high-speed isothermal jets are presented in Sec. III. The contribution of sub-optimal modes to the far-field noise is measured, and their role in noise generation is discussed in detail. We repeat input-output analysis for 13 Reynolds-averaged Navier-Stokes (RANS) solutions spanning a range of different jet Mach numbers. The relevance of sub-optimal modes is further assessed through analysis of unsteady LES data. In Sec. IV, we demonstrate that our results do not depend on grid resolution or the choice of input and output domains. Finally, Sec. V summarizes the conclusions of this study.

II. METHODOLOGY

A. Base flows

We consider infinitesimal perturbations about RANS solutions of ideally expanded, axisymmetric, compressible, turbulent jets (Fig. 1). A white line from $x/R = -20$ to $x/R = 0$ in Fig. 1

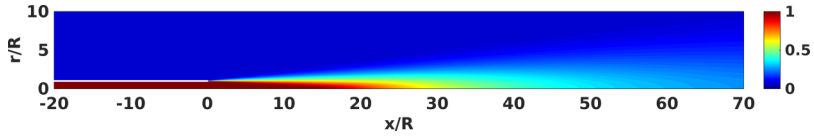

FIG. 1. Contours of axial velocity from a RANS solution of a round $M_j = 1.5$ supersonic jet. The velocity contours are normalized by the velocity at the nozzle exit at $x/R = 0$. The cylindrical nozzle is represented by the white line extending from $x/R = -20$ to $x/R = 0$ at $r/R = 1$.

corresponds to a straight cylindrical nozzle with radius $R = 1$ and wall thickness $t = 0.3R$. The RANS solutions are computed using a modified $k - \varepsilon$ turbulence model with coefficients suggested by Thies and Tam[30] for high-speed jets. A RANS solution for a $M_j = 1.5$ jet corresponds to the operating conditions of an LES performed previously,[31] including a weak co-flow surrounding the main jet. The magnitude of the co-flow in this case is set to 6.7% of nozzle exit velocity and this co-flow is enforced at the upstream boundary outside of the nozzle. In addition to the RANS solution for the $M_j = 1.5$ jet, we also produce RANS solutions over a range of jet Mach numbers. In each case, we consider ideally expanded and isothermal jets such that $T_j/T_\infty = 1$, $p_j/p_\infty = 1$, and the Reynolds number $Re = \rho_j u_j R/\mu = 10^6$, where μ is the dynamic viscosity, which we assume to be constant throughout the domain. Here, the subscripts j and ∞ represent properties at the nozzle exit and in the ambient fluid, respectively. The computational domain extended from $x/R = -20$ to $x/R = 70$ in the axial direction and from $r/R = 0$ to $r/R = 50$ in the radial direction.

B. Governing equations

The Euler equations govern the dynamics of the system state $\mathbf{q} = \left[p;\, \mathbf{u}^T;\, s\right]^T$, where p, $\mathbf{u}$, and s are the fluid pressure, velocity, and entropy, respectively. After non-dimensionalization with respect to the nozzle radius R, the jet velocity u_j, density ρ_j, and temperature T_j at the nozzle exit, these equations are written as

$$\frac{\partial p}{\partial t} + \mathbf{u}\cdot\nabla p + \rho c^2 \nabla\cdot\mathbf{u} = 0, \tag{1}$$

$$\frac{\partial \boldsymbol{u}}{\partial t} + \frac{1}{\rho}\nabla p + \boldsymbol{u}\cdot\nabla\boldsymbol{u} = 0, \tag{2}$$

$$\frac{\partial s}{\partial t} + \boldsymbol{u}\cdot\nabla s = 0. \tag{3}$$

Here, the entropy is defined by

$$s = \ln(T)/((\gamma-1){M_j}^2) - \ln(p)/(\gamma {M_j}^2) \tag{4}$$

so that $s = 0$ is satisfied when $p = 1$ and $T = 1$.[18,32] With this non-dimensionalization, the equation of state for an ideal gas becomes $\gamma {M_j}^2 p = \rho T$. The jet Mach number is defined as $M_j = u_j/c_j$ in terms of the speed of sound at the nozzle exit $c_j = \sqrt{\gamma p_j/\rho_j}$, where the ratio of specific heats γ has constant value 1.4.

To examine the behavior of small fluctuations about the base flows, the Euler equations (1)-(3) are linearized. By decomposing the system state $\boldsymbol{q}$ into mean $\bar{()}$ and fluctuating parts $()'$, i.e., $\boldsymbol{q} = \bar{\boldsymbol{q}} + \boldsymbol{q}'$ and neglecting higher-order terms, we obtain the homogeneous linearized Euler equations (LEE),

$$\frac{\partial p'}{\partial t} + \bar{\boldsymbol{u}}\cdot\nabla p' + \bar{\rho}\bar{c}^2\nabla\cdot\boldsymbol{u}' + \gamma(\nabla\cdot\bar{\boldsymbol{u}})p' = 0, \tag{5}$$

$$\frac{\partial \boldsymbol{u}'}{\partial t} + \frac{1}{\bar{\rho}}\nabla p' + \bar{\boldsymbol{u}}\cdot\nabla\boldsymbol{u}' + \boldsymbol{u}'\cdot\nabla\bar{\boldsymbol{u}} = 0, \tag{6}$$

$$\frac{\partial s'}{\partial t} + \bar{\boldsymbol{u}}\cdot\nabla s' + \boldsymbol{u}'\cdot\nabla\bar{s} = 0. \tag{7}$$

In matrix form, the LEE can be written as

$$\frac{\partial q}{\partial t} = Aq, \tag{8}$$

where q is the perturbation state and the linear operator A depends on the base flow. For simplicity, we have dropped the primes and bold font.

C. Input-output analysis

The stability of linearized system (8) can be analyzed using the wavelike modal decomposition for perturbations,

$$q(x,r,\theta,t) = \hat{q}(x,r)e^{i(m\theta-\omega t)}, \tag{9}$$

where m is an integer azimuthal wavenumber and ω is the temporal frequency. The scope of this study is limited to axisymmetric disturbances with $m = 0$.

The high-speed jets that are considered in the present study are globally stable; all zero group velocity modes decay in time. They are, however, highly unstable to convective perturbations in the form of wavepackets.[16] We therefore treat these jets as amplifiers which take external disturbances as inputs and give back far-field acoustics as outputs. This behavior is much different from that of globally unstable flows, which support self-sustained oscillations.

To understand how inputs map to outputs, we rewrite the original linear system (8) in the presence of an external forcing f,

$$\dot{q} = Aq + Bf, \tag{10}$$

$$y = Cq, \tag{11}$$

with y being quantities of interest, i.e., noise in our study. Here, B and C are matrices that are chosen to specify inputs and outputs of interest.

The above system yields a transfer function H from inputs $f = \hat{f}e^{zt}$ to outputs $y = \hat{y}e^{zt}$ for a given temporal frequency ω as

$$H = C(zI - A)^{-1}B, \tag{12}$$

where $z = -i\omega$. Using singular value decomposition (SVD) at each ω, H may be further decomposed as

$$H = U\Sigma V^* \quad \text{or} \quad HV = U\Sigma. \tag{13}$$

Here, U and V are unitary matrices, Σ is a matrix whose diagonal consists of singular values, and $(\,)^*$ denotes the complex-conjugate transpose. Thus, the system is interpreted such that each column of V is an input vector that is mapped to the corresponding column of U through the transfer function H.[26] The corresponding singular value represents the gain in amplitude from input to output, defined by

$$\sigma = \frac{\|y\|}{\|f\|}, \tag{14}$$

where $\|\cdot\|^2 = \langle\cdot,\cdot\rangle$ with an inner product defined as

$$\langle q_1, q_2\rangle \equiv \int_V q_1^* q_2 dV. \tag{15}$$

For disturbances with azimuthal wavenumber $m = 0$, the differential volume element in cylindrical coordinates is given by $dV = 2\pi r dr$. With respect to this inner product, the adjoint A^+ of the linear operator is defined by

$$\left\langle A^+ q_1, q_2\right\rangle = \langle q_1, Aq_2\rangle, \tag{16}$$

where q_1 and q_2 are any two state vectors. After discretization, we can represent this in matrix form as

$$(A^+ q_1)^* W q_2 = q_1^* W A q_2, \tag{17}$$

where W is a real diagonal matrix of quadrature weights. This implies that the adjoint of a discretized version of the operator A is

$$A^+ = W^{-1}A^*W. \tag{18}$$

We use these definitions to find the singular values and the right-singular vectors of H through the eigenvalue decomposition of H^+H

$$H^+H = B^*(z^*I - A^*)^{-1}C^*C(zI - A)^{-1}B. \tag{19}$$

Here, the eigenvalues of H^+H are the squares of the corresponding singular values σ of H.

The adjoint of the transfer function H^+, which maps outputs back onto inputs, may be evaluated in two different ways. As written above, the discrete adjoint approach first discretizes the continuous equations and then derives the adjoint through a matrix transpose. Alternatively, in the continuous adjoint approach, equations adjoint to the LEE are first derived through integration by parts and then discretized later to find a matrix that approximates A^*. The continuous adjoint approach, however, allows specification of one-sided differences consistent with continuous derivatives near to wall boundaries, such as the cylindrical nozzle. The discrete approach, on the other hand, does not guarantee consistency near boundaries, resulting in large numerical errors. For this reason, we adopt the continuous adjoint approach in the present investigation.[33–36]

One advantage of input-output analysis is that the matrices B and C may be selected depending on inputs and outputs of interest. For example, in the present study, we have chosen B to force the velocity equation (6) in the immediate vicinity of jet ($r/R < 2.90$) and C to select far-field pressure ($r/R > 8.70$). The spatial separation of input and output domains is motivated in part by the acoustic analogy approach[1,5] where acoustic sources are separated from acoustic propagation through an exact rearrangement of the compressible Navier-Stokes equations. In this view, acoustic sources are associated with unsteady turbulent flow and thus are restricted in space to the immediate vicinity of the jet. The effects, however, occur far away from the jet where acoustic propagation is important, but acoustic sources are inactive. Recently, statistical models of acoustic source terms, calibrated by high-fidelity simulation data and laboratory measurements, have been shown to successfully predict noise from high-speed jets after convolution with an appropriate adjoint Green's function.[7,37] The present analysis is in concert with this idea, but instead of analyzing two-point two-time fourth order statistical correlations, we use input-output analysis of the linearized equations to identify dynamic structure in the acoustic sources.

D. Numerical methods

The LEE are discretized by fourth-order centered finite differences on a stretched mesh in cylindrical coordinates, yielding a large sparse matrix. Since the centered finite difference scheme is non-dissipative, a weak scale-selective fourth-order numerical filter is added to damp unphysical waves at the highest wavenumbers. To approximate the Sommerfeld radiation condition, numerical sponge layers[38,39] are employed at the upstream, downstream, and lateral boundaries. As discussed below, we repeat our calculations on a range of different grid resolutions to ensure that our results are independent of the discretization.

The largest eigenvalues of H^+H are computed using the implicitly restarted Arnoldi method (IRAM) as implemented by the software package ARPACK.[40] We compute the matrix inversion associated with the resolvent operator using the sparse direct solver PARDISO which is part of the Intel math kernel library. Because the iterative Arnoldi method requires many evaluations of the resolvent at a fixed frequency, the matrix $zI - A$ may be factorized only once. After this, the factors are applied to efficiently perform repeated evaluations of the resolvent. Compared to global mode analysis where non-normality of the system matrix A may impede convergence of the Arnoldi method, the eigenvectors of H^+H form an orthonormal set of input modes, so the Arnoldi method converges rapidly.

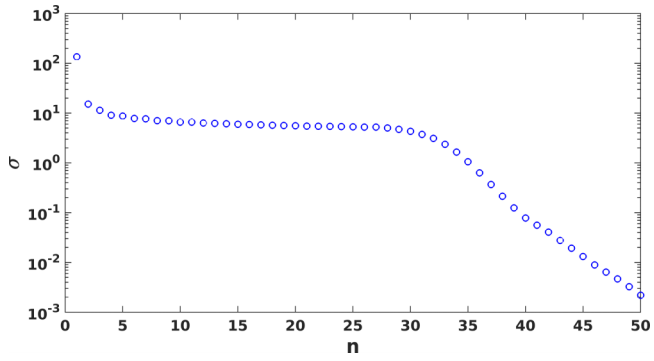

FIG. 2. Singular values vs. mode number for the $M_j = 1.5$ supersonic jet with forcing frequency $St = 0.33$.

III. RESULTS

A. Optimal and sub-optimal modes

At every temporal frequency ω, we obtain orthonormal sets of input and output modes, ordered by the corresponding gains. In what follows, we denote this ordering by the mode number n. Figure 2 shows the first 50 gains for the $M_j = 1.5$ supersonic jet at frequency $St = 2Rf/u_j = 0.33$, where $f = \omega/(2\pi)$. Mode number $n = 1$ is associated with the maximum gain, which was found to be $\sigma_1 = 1.35 \times 10^2$. Figure 3(a) shows the corresponding optimal forcing mode and Fig. 4(a) shows the resulting output mode. As indicated by the rectangle in Fig. 3, we have restricted the input forcing to be inside the region $-10 < x/R < 60$ and $0.29 < r/R < 2.90$. The output, however, is restricted to be pressure perturbations inside the region $-10 < x/R < 60$ and $8.70 < r/R < 39.2$, as indicated by the rectangle in Fig. 4(a). This choice is motivated by the goal of understanding how forcing the velocity equations inside the jet produces sound in the far-field. To avoid numerical errors due to sharp transitions at the boundaries of the input and output domains, input modes are gradually reduced to zero over several grid points.

The input modes are visualized by contours of the real part of the input axial velocity forcing restricted in the near-field, and the output modes are visualized by contours of the real part of the output pressure in the far-field. For this supersonic jet, the output pressure agrees well with the acoustic far-field of a wavepacket computed using PSE or global mode analysis. It consists of a single acoustic beam radiating at an angle of 30° in the direction of peak jet noise. We also observe that the input is mostly concentrated near the nozzle lip. For supersonic jets, instability waves are

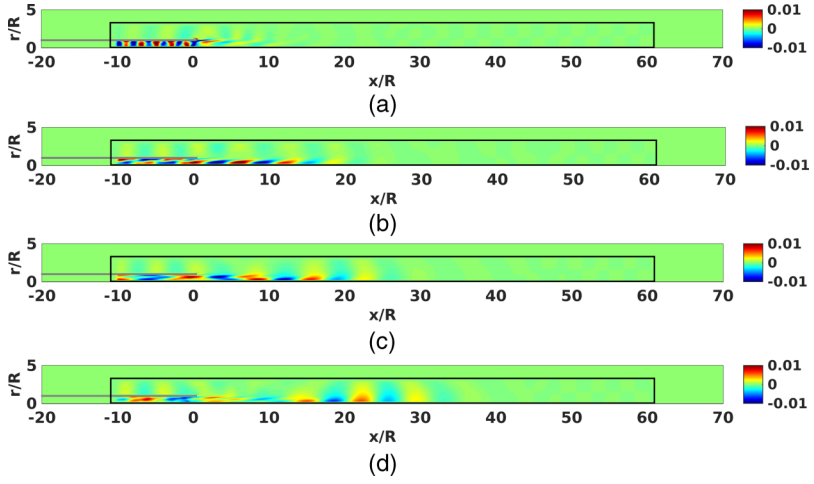

FIG. 3. The first four input modes of the $M_j = 1.5$ supersonic jet for forcing frequency $St = 0.33$. Contours of the real part of the normalized axial velocity forcing are shown. (a) $n = 1$. (b) $n = 2$. (c) $n = 3$. (d) $n = 4$.

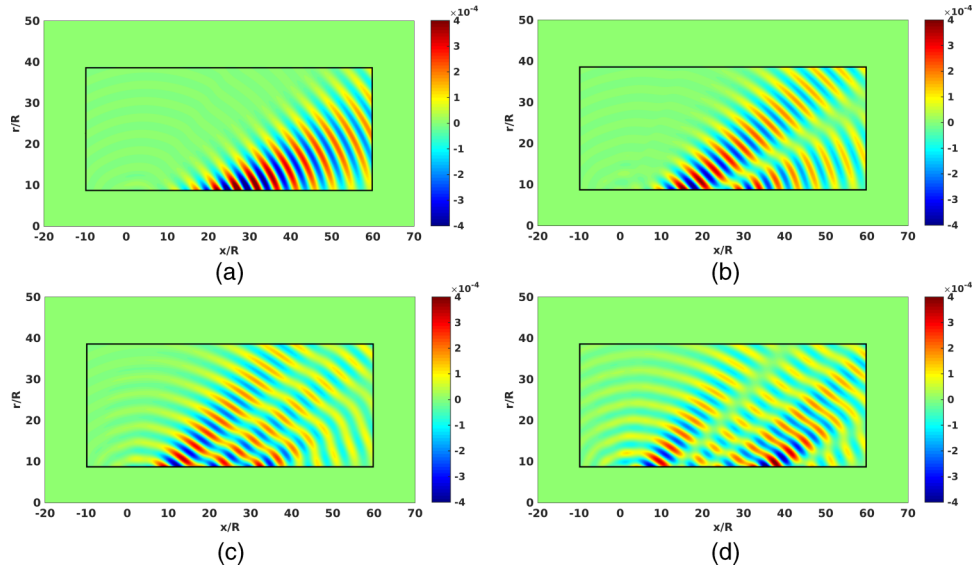

FIG. 4. The first four output modes of the $M_j = 1.5$ supersonic jet for forcing frequency $St = 0.33$. Contours of the real part of normalized output pressure fluctuations are shown. (a) $n = 1$. (b) $n = 2$. (c) $n = 3$. (d) $n = 4$.

linked to the acoustic far-field through the Mach wave mechanism.[41] According to this mechanism, a small disturbance upstream can trigger a supersonic instability wave downstream which then generates noise. This instability process is captured well by the PSE.[14]

In addition to the optimal mode, input-output analysis of jet noise yields several sub-optimal modes. These sub-optimal modes follow a pattern as shown in Fig. 4. Whereas the optimal output mode ($n = 1$) consists of a single acoustic beam, the first sub-optimal output mode ($n = 2$) is comprised of two acoustic beams radiating away from the jet. Note that in the first sub-optimal mode, one beam radiates at a slightly larger angle with respect to the centerline than does the single beam in the optimal mode. The other acoustic beam in the first sub-optimal mode propagates at a slightly smaller angle with respect to the centerline than the single beam in the optimal mode. Similarly, the third output mode ($n = 3$) contains three acoustic beams: one at a yet larger radiation angle, one at a smaller radiation angle, and one at an intermediate angle. These three acoustic beams follow the edges of the two acoustic beams associated with the first sub-optimal mode. The higher modes continue to follow this tendency of incorporating additional beams that radiate at larger angles with respect to the downstream jet axis.

While the optimal input mode is concentrated inside the nozzle and at the jet exit, the sub-optimal input mode shapes shown in Fig. 3 extend increasingly far downstream as the mode number increases. For $n = 4$, the peak input forcing is located at $x/R \approx 20$ downstream inside the jet.

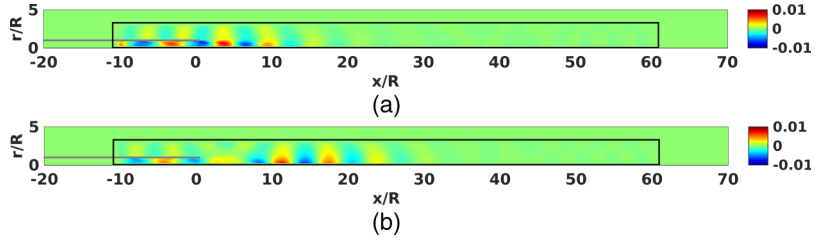

FIG. 5. The first two input modes of the $M_j = 0.9$ subsonic jet for forcing frequency $St = 0.56$. Contours show the real part of axial velocity forcing as in Fig. 3. (a) $n = 1$. (b) $n = 2$.

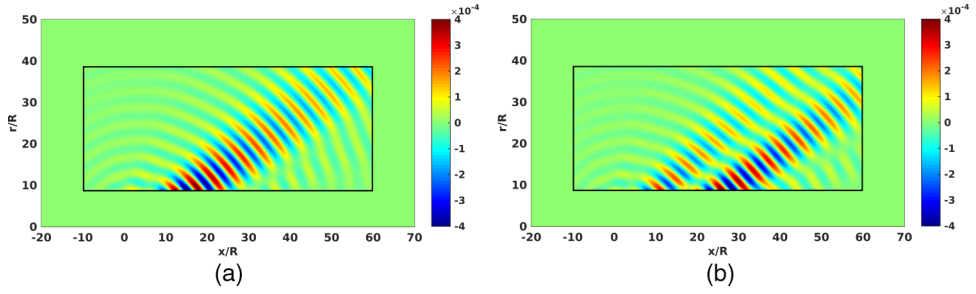

FIG. 6. The first two output modes of the $M_j = 0.9$ subsonic jet for forcing frequency $St = 0.56$. Contours show the real part of pressure fluctuations as in Fig. 4. (a) $n = 1$. (b) $n = 2$.

B. Effect of jet Mach number

To investigate the effect of jet Mach number on the role of the sub-optimal modes, we repeat the input-output analysis for a $M_j = 0.9$ isothermal jet with forcing frequency $St = 0.56$. As discussed below, this jet Strouhal number yields the same acoustic Strouhal number $St_a = StM_a = 0.50$, where $M_a = u_j/c_\infty$ is the acoustic Mach number defined in terms of the ambient speed of sound, c_∞. For isothermal jets, $c_\infty = c_j$, so $M_a = M_j$. Figures 5 and 6 show the first two input and output modes, respectively. In contrast to the supersonic jet, the optimal input for the subsonic jet extends farther downstream from the nozzle exit. The output modes, however, follow a similar pattern to the supersonic case. The optimal mode has a single acoustic beam radiating away from the jet, while the second mode (first sub-optimal) has an additional beam. The radiation angles for the subsonic jet output modes are greater than for the supersonic case.

Figure 7 shows singular values for the $M_j = 0.9$ subsonic jet. For the supersonic jet, the largest singular value, representing the maximum gain by the optimal mode, was two orders of magnitude greater than the gain obtained for the first sub-optimal mode. In the subsonic jet, however, the second singular value is comparable to the most significant singular value. This suggests that while the optimal mode dominates the acoustics in the supersonic jet, the contribution of sub-optimal modes should not be neglected in predicting the subsonic jet noise.

To quantify the importance of the sub-optimal modes, note that the sum of the squares of the singular values is proportional to the total acoustic intensity of output modes in response to white noise forcing. The acoustic intensity of the optimal output mode is proportional to the square of the first singular value, alone. Therefore, the decibel increase in sound pressure level (ΔSPL) obtained by including the sub-optimal modes vs. retaining only the optimal mode is

$$\Delta SPL = 10 \log_{10}\left(\frac{\sum \sigma_i^2}{\sigma_1^2}\right). \tag{20}$$

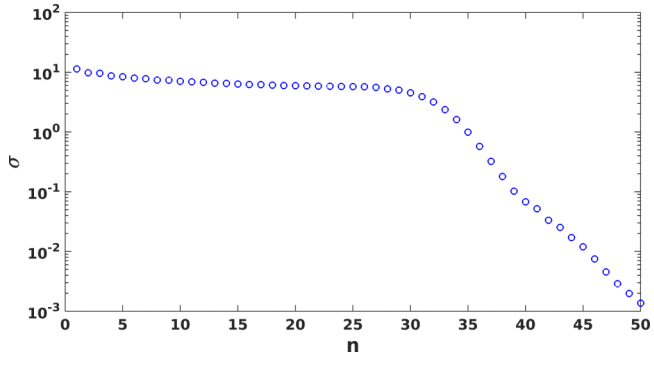

FIG. 7. Singular values vs. mode number for the $M_j = 0.9$ subsonic jet with forcing frequency $St = 0.56$.

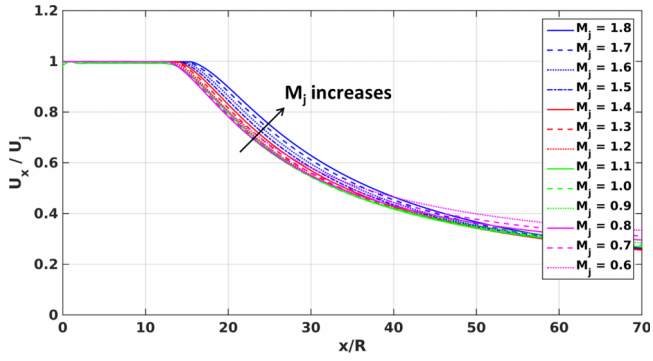

FIG. 8. Streamwise distribution of axial velocity on the jet centerline.

For the supersonic jet at $St_a = 0.50$, we find a marginal increase of 0.33 dB, owing to the dominance of the optimal mode. For the subsonic case, however, including the sub-optimal modes resulted in a 10.6 dB increase in SPL.

In addition to the $M_j = 0.9$ and $M_j = 1.5$ jets, we computed 11 other RANS base flows corresponding to high-speed isothermal jets. The entire database covers jet Mach numbers ranging from $M_j = 0.6$ to 1.8 in increments of 0.1. Figure 8 compares centerline axial velocity for these base flows. Note that the potential core length increases slightly with increasing jet Mach number.

Figure 9 shows singular values for several subsonic and supersonic jets at the same jet Strouhal number $St = 0.33$. The singular values suddenly drop after a certain mode number, and this sudden decrease is delayed with increasing jet Mach number. For example, the singular values drop after $n \approx 15$ for the $M_j = 0.9$ subsonic jet and $n \approx 30$ for the $M_j = 1.5$ supersonic jet, respectively.

We find, however, that many of the sub-optimal singular values collapse to a single curve if we fix the acoustic Strouhal number St_a instead of the jet Strouhal number St. The acoustic Strouhal number controls the wavelength of acoustic waves outside of the jet. Figure 10 shows singular values for a number of different jet Mach numbers for fixed acoustic Strouhal number $St_a = 0.50$. This result implies that the acoustic Strouhal number may be used as a new scale to anticipate the sudden drop of gains in the input-output behavior of jet noise.

While many of the singular values collapse for fixed St_a, the optimal mode and first few sub-optimal modes remain sensitive to jet Mach number. Here, we again observe that the first singular value dominates the response of supersonic jets, whereas sub-optimal modes play a more significant role for subsonic jets. Using Equation (20), Fig. 11 shows the increase in SPL owing to sub-optimal modes as a function of jet Mach number. We interpret the drop in ΔSPL at $M_j \approx 1.3$ to be a consequence of the onset of Mach wave radiation. Assuming that the optimal mode corresponds to an instability wavepacket with convection velocity u_c between $0.65u_j < u_c < 0.8u_j$,[21,41] then we can expect the onset of Mach wave radiation to occur between $1.3 < M_a < 1.6$. Mach wave radiation occurs when disturbances propagate along the jet supersonically with respect to the

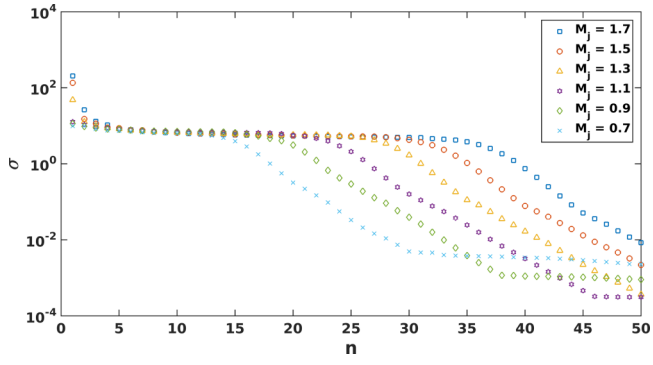

FIG. 9. Singular values *vs*. mode number for different jet Mach numbers keeping the jet Strouhal number fixed $St = 0.33$.

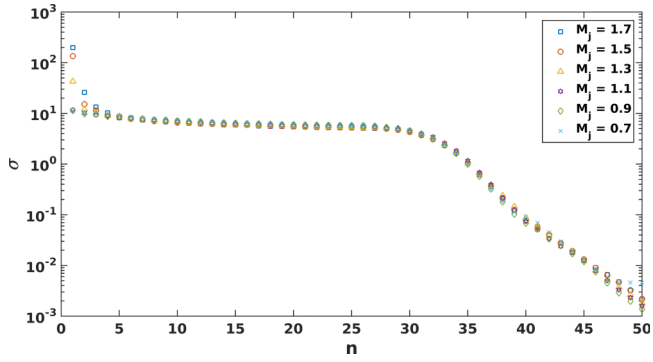

FIG. 10. Singular values *vs.* mode number for different jet Mach numbers keeping the acoustic Strouhal number fixed $St_a = 0.50$.

ambient speed of sound, coupling near-field pressure disturbances to far-field acoustic radiation in a linear fashion.[41]

C. Amplitudes of sub-optimal modes

Since input-output analysis is linear, the amplitudes of the input and output modes are arbitrary and are in fact normalized with respect to inner product (15). As previously noted, the increase in noise ΔSPL shown in Fig. 11 assumes that all modes are forced equally with unit energy. In other words, this assumes that the forcing supplied by the jet turbulence to the input modes is equivalent to white noise. It is well-known, however, that the statistics of turbulent fluctuations are not equivalent to white noise. In this section, we therefore investigate whether the sub-optimal modes remain relevant when realistic forcing from an LES is projected onto their input singular directions.

For this purpose, an LES database for an isothermal jet with jet Mach number $M_j = 1.5$ and 6.7% axial co-flow was obtained using an unstructured finite-volume compressible flow solver. For further details about this LES, we refer the reader to Brès *et al.*[31] The LES base flow was computed as the time average of 10 000 snapshots taken from the LES spaced at time intervals of $0.02D/c_\infty$. Since we consider an axisymmetric jet in the present study, the base flow is also averaged in the azimuthal direction. Figure 12 shows contours of axial velocity for the base flow taken from the LES.

Compared to the RANS calculations, the LES was conducted for a smaller numerical domain, ranging from $x/R = 0$ to 40 and $r/R = 0$ to 10, in the axial and lateral directions, respectively. The LES base flow was extrapolated to the RANS domain so that input-output analysis using both base flows could be appropriately compared. Considering the spatial restriction of the original LES domain, we also restricted the input and output domains to $x/R = 40$ in the streamwise direction,

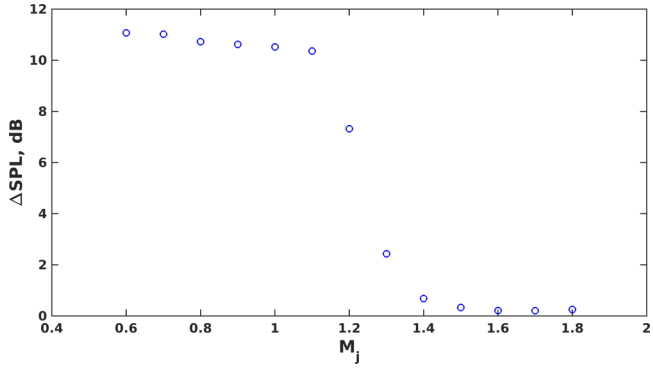

FIG. 11. Noise increase including sub-optimal modes with respect to the jet Mach number.

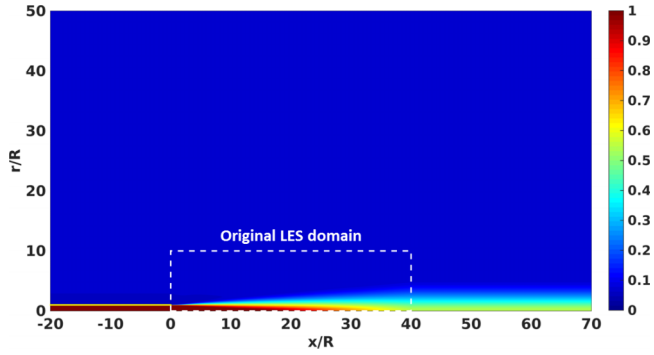

FIG. 12. Contours of time-averaged axial velocity from a LES of a $M_j = 1.5$ supersonic jet. The white dashed lines indicate the extent of the computational domain of the LES. As discussed in the text, the resulting base flow was then extended to the larger domain used for calculations based on RANS solutions.

but other parameters remained unchanged. Due to slightly mismatched conditions between two base flows, an exact comparison is not possible. Nevertheless, the singular values for both cases agree remarkably well, as shown in Fig. 13. The only discrepancy is observed for the first singular value, which is 1.77 times larger for the LES base flow than for the RANS base flow. We note, however, that the singular directions (not shown) for these two cases are nearly identical.

The discrepancy in optimal gain is in part related to the convergence levels of the RANS and LES base flows. Since RANS calculations are not computationally expensive, they are converged to machine precision. On the other hand, even though the LES base flow is formed from an average of 10 000 snapshots, small residual errors remain that are larger than those associated with RANS. Therefore, the LES base flow is less smooth than the RANS base flow, with enhanced spatial gradients leading to enhanced gain. Confirming this, we also find that averaging fewer snapshots leads to a slightly greater optimal gain. The input and output modes, however, remain essentially unchanged. The robustness of the input and output modes highlights the fact that input-output analysis does not rely upon an assumption of a smoothly varying base flow. In other words, a useful feature of input-output analysis is that it can be applied directly to "noisy" base flows and still yield reasonable results — results that become increasingly accurate as the convergence of the base flow improves.

Another source of the discrepancy in optimal gain between RANS and LES may be the fact that the shear layers in the LES emerge from the nozzle in an initially laminar state. As documented by Brès *et al.*,[31] this leads to an overshoot in fluctuation levels close to the nozzle lip compared to experimental measurements. Large gradients associated with thin initial shear layers increase the growth of instability waves, and thus increase the optimal gain in the present analysis. The RANS calculations, on the other hand, use a modified $k-\varepsilon$ model that is known to produce base flows that validate well against experiment. Nevertheless, to be conservative, we choose to use the LES

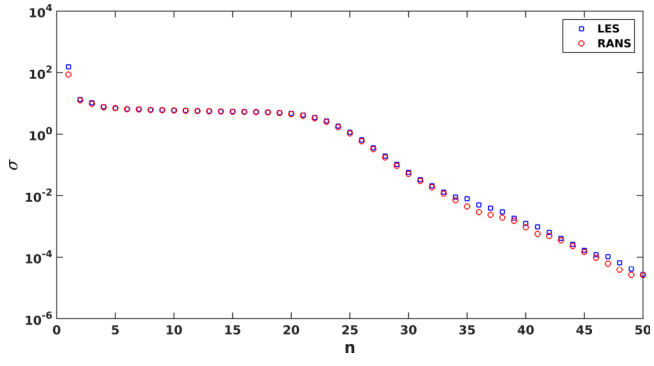

FIG. 13. Spectra of singular values using the RANS and LES base flows for $M_j = 1.5$ at $St = 0.33$.

base flow specifically because it represents the worst case. The difference in gains between optimal and sub-optimal modes is greater for the LES base flow, so the importance of sub-optimal modes appears diminished. The results obtained below, however, should be seen as lower bounds.

The input forcing f we consider in this paper appears as a source term added to the right hand side of the linearized velocity equation (6). This source term can also be derived through an exact rearrangement of Equation (2). Substituting $\boldsymbol{u} = \bar{\boldsymbol{u}} + \boldsymbol{u}'$ and $\rho = \bar{\rho} + \rho'$ into Equation (2), subtracting out base flow terms, and collecting terms associated with the linearized operator A on the left hand side yield

$$\frac{\partial \boldsymbol{u}'}{\partial t} + \frac{1}{\bar{\rho}}\nabla p' + \bar{\boldsymbol{u}} \cdot \nabla \boldsymbol{u}' + \boldsymbol{u}' \cdot \nabla \bar{\boldsymbol{u}} = \left[\frac{1}{\bar{\rho}} - \frac{1}{\bar{\rho} + \rho'}\right] \nabla p' - \boldsymbol{u}' \cdot \nabla \boldsymbol{u}'. \tag{21}$$

Note that this is exactly the same procedure used to derive an acoustic analogy. After taking Fourier transforms in time and in the azimuthal direction, the nonlinear source term simplifies to

$$\hat{q}_{LES} = FFT\left(\frac{\rho' \nabla p'}{\bar{\rho}(\bar{\rho} + \rho')} - \boldsymbol{u}' \cdot \nabla \boldsymbol{u}'\right). \tag{22}$$

To evaluate the physical relevance of the optimal and sub-optimal input modes resulting from our analysis, we compute this source term directly from high-fidelity LES data. The input modes are physically relevant if they capture at least a portion of the spatio-temporal behavior of the LES forcing. This is quantified by projecting the LES forcing onto the basis of input modes,

$$a_n = \left\langle \hat{q}_{LES}, q_{in,n} \right\rangle. \tag{23}$$

Here, a_n denotes the amplitude of input mode $q_{in,n}$ in the LES forcing. Figure 14 shows amplitudes $|a_n|$ resulting from this process at forcing frequency $St = 0.33$ and azimuthal wavenumber $m = 0$. Here, the amplitudes are normalized by the average amplitude of the LES source. Overall, less than 0.3% of the energy contained in the LES source is projected onto the input modes. This agrees with the observation that only a small fraction of the overall aerodynamic energy in a turbulent jet is ever radiated as sound.[42] We also note that the amplitudes of many sub-optimal modes are larger than the amplitude of the optimal mode. This indicates that sub-optimal input modes are physically relevant and should not be neglected.

To quantify the effect of sub-optimal input modes, we use effective gains by modulating the white-noise gains by the amplitudes resulting from the LES projection,

$$\sigma_{eff,n} = \sigma_n a_n. \tag{24}$$

The total energy in the output is computed as the sum of squares of the effective gains, resulting in a total increase in the output SPL of 0.53 dB by including the sub-optimal modes. Because the decibel scale is logarithmic, this represents a significant increase compared to $\Delta SPL = 0.16$ dB, obtained with white noise forcing. In summary, we find sub-optimal modes to be even more relevant in the presence of realistic forcing than they are in the case of white noise forcing.

To assess the physical relevance of output modes, we compare them to the acoustic far-field predicted by the LES.[43] For this purpose, we employ the Kirchhoff method to project near-field pressure fluctuations from the LES outwards, away from the jet.[11] This is necessary because the

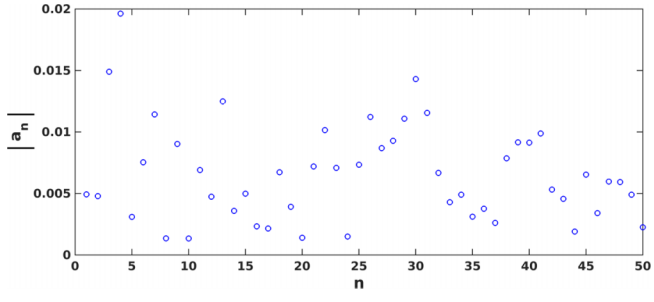

FIG. 14. Amplitudes $|a_n|$ determined by projecting the LES forcing onto the basis of input modes for $M_j = 1.5$ at $St = 0.33$.

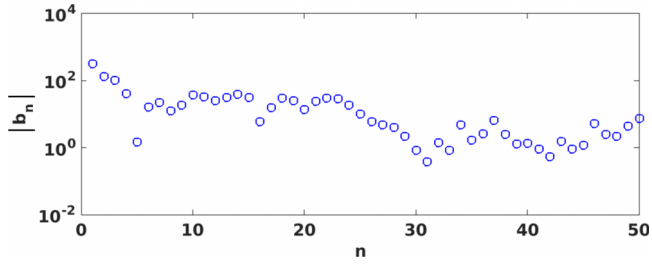

FIG. 15. Amplitudes $|b_n|$ determined by projecting LES acoustic field onto the orthonormal basis of output modes.

LES domain is smaller than the domain considered for the output modes. After computing the acoustic field associated with the LES over the entire output domain, this field is then projected onto the orthogonal set of output modes. Similar to Equation (23), amplitudes associated with output modes are determined by

$$b_n = \left\langle p_{LES}, p_{out,n} \right\rangle . \tag{25}$$

Figure 15 shows the amplitudes $|b_n|$ vs. output mode number. For this supersonic jet, we find that optimal output mode is most prevalent in the LES acoustic data. As shown in Fig. 4, the optimal mode consists of a single acoustic beam at the Mach wave angle. From Equation (25), we find that this mode accounts for 57% of the acoustic energy in the output domain.

By including more output modes, we recover even more of the acoustic output energy. Figure 16 shows the dependence of the recovered acoustic energy on the number of retained output modes. A superposition of 24 output modes recovers almost 70% of the acoustic energy of the LES. Therefore, even though the input modes capture only a small portion of the nonlinear source term, the acoustic field of the corresponding output modes reliably captures the results of a nonlinear simulation. This implies that the input modes must indeed capture the small, but radiating portion of the nonlinear source term.

While the output modes successfully recover a large portion of the acoustic energy, the agreement is not perfect. Because input-output analysis is linear, possible nonlinear interactions between input modes leading to far-field sound are neglected. Also, by restricting the input forcing to the velocity equation (6), we neglect forcing applied to the pressure equation (5) which also may lead to far-field sound. In other words, a part of the LES acoustic field may arise from sources that are not present in our current formulation. Nevertheless, it is striking that 70% of the acoustic energy can be recovered by introducing forcing only to the linearized velocity equations.

Figure 16 shows that including more than 24 output modes in the superposition has little effect on how well the LES acoustic field is approximated. Mode number 24 also coincides with the drop off in gains shown in Fig. 13. This implies that an input-output system comprised of just 24 modes is sufficient to represent the noise generation mechanisms in an $M_j = 1.5$ jet at frequency $St = 0.33$ and azimuthal wave number $m = 0$. This offers a substantial reduction compared to the spatial discretization of the original system of equations having almost a half-million degrees of freedom. This information can be used to obtain reduced-order models of noise generation.

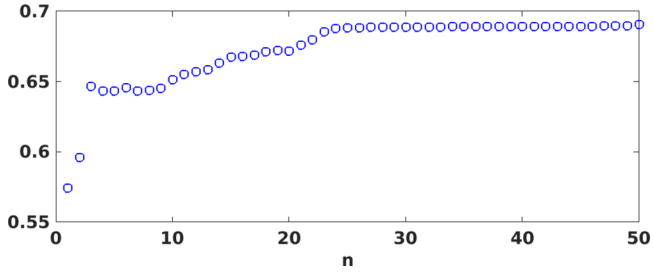

FIG. 16. Recovered acoustic energy as a function of number of retained output modes.

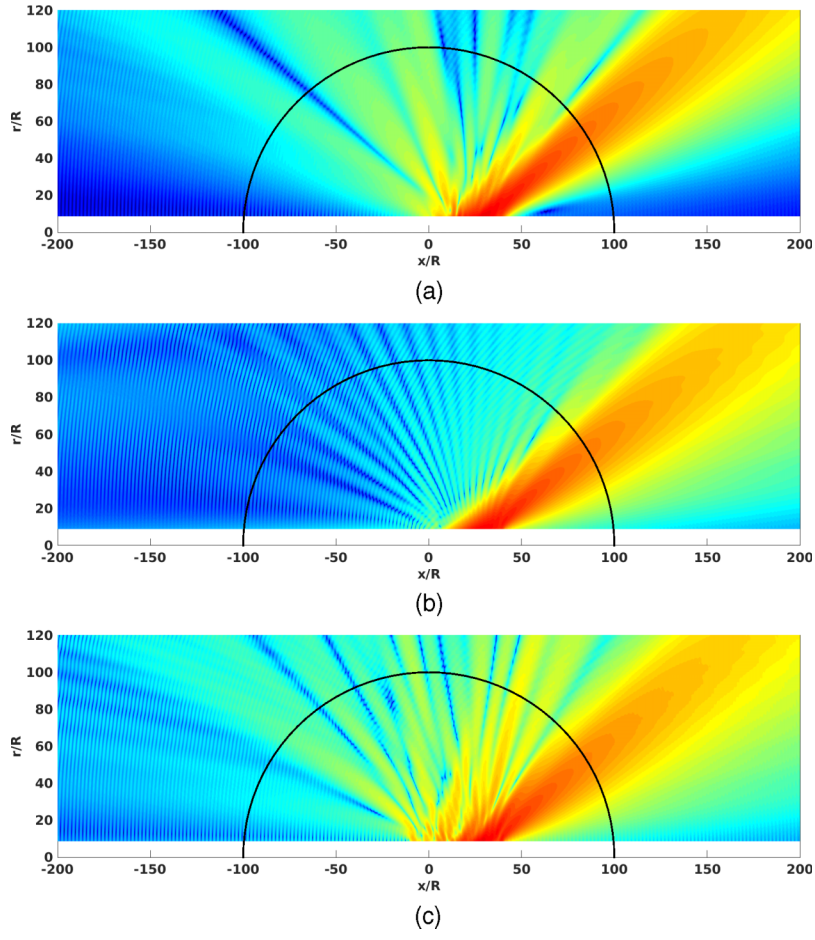

FIG. 17. Contours of decibel levels of (a) the LES acoustic field, (b) the acoustic field of the first output mode alone, and (c) an acoustic field reconstructed from a superposition of 24 output modes. The black arc indicates a distance of 100 jet radii away from the center of the jet nozzle.

To further understand the effect of including sub-optimal modes on the acoustic far-field, we use the Kirchhoff method to project both the LES data and the superposition of 24 output modes yet further into the far-field. Figures 17(a) and 17(c) show the decibel levels as a function of axial and radial positions for the LES and output-mode-reconstructed acoustic field, respectively. The black circular arc indicates a distance of 100 jet radii away from the nozzle exit. Figure 17(b) shows an acoustic field reconstructed from only the first output mode. An acoustic beam at the Mach wave angle is visible in all three figures. Sideline and upstream acoustic radiation are markedly absent,

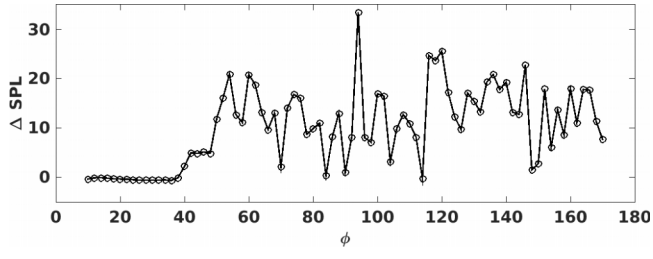

FIG. 18. Increase in far-field sound pressure levels owing to sub-optimal modes as a function of polar angle ϕ from the downstream jet axis.

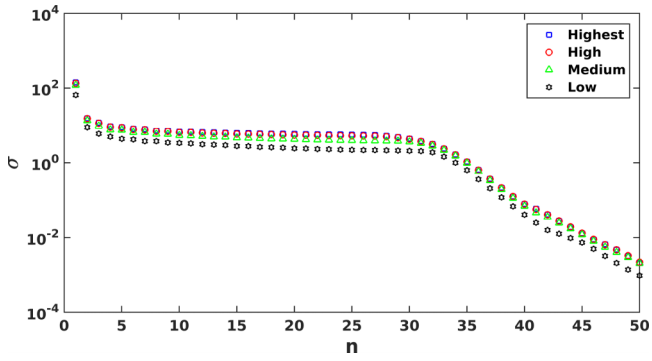

FIG. 19. Singular values using four different grid resolutions for the $M_j = 1.5$ supersonic jet at $St = 0.33$.

however, from Fig. 17(b). Clearly, inclusion of the sub-optimal modes recovers this missing sideline and upstream sound, in good agreement with the LES acoustic field.

We quantify this contribution of the sub-optimal modes in Fig. 18 by plotting the SPL difference between the fields shown in Figs. 17(b) and 17(c) as a function of polar angle ϕ from the downstream jet axis along the black circular arc. We find that for $\phi > 40°$, sub-optimal modes account for a 10–20 dB increase over levels of the optimal mode alone. We therefore conclude that sub-optimal modes are associated with sideline noise. Unlike stochastic models,[44] however, the sideline noise created by sub-optimal modes arises from coherent motions. Furthermore, owing to the similarities between Figs. 17(a) and 17(c), we suggest that a large part of sideline noise can be explained by such coherent motions embedded in the jet.

In summary, projection of LES source term data onto input modes and the LES acoustic far-field onto output modes has demonstrated that both types of modes are physically relevant. We also found that input-output analysis reveals the minimum dimensionality required of reduced-order models to accurately represent the mechanisms of acoustic generation. Finally, in comparison to the optimal output mode, we have found that sound recovered by sub-optimal modes is directed mostly in the sideline and upstream directions. As such, sub-optimal modes provide a new interpretation of sideline noise in terms of coherent motions.

IV. DISCUSSION

A. Grid independence

Four different grid resolutions are tested to study the convergence of input-output analysis. For each resolution, grid points are distributed uniformly in the streamwise direction but are refined and stretched in the lateral direction to cluster grid points along the nozzle lip line. Figure 19 shows singular values for the $M_j = 1.5$ supersonic jet for the four different grid resolutions. For sufficiently high grid resolutions, the singular values do not change significantly. We quantify this convergence in Table I which lists the magnitude of the largest singular value along with the percentage of

TABLE I. Optimal singular values, sub-optimal energy percentages, and convergence factors for four different grid resolutions for the $M_j = 1.5$ supersonic jet for forcing frequency $St = 0.33$.

Label	N_x	N_r	σ_1	$\frac{\sum\sigma^2_{sub-optimal}}{\sum\sigma^2_{total}}$	Convergence factor
Low	256	128	6.56×10^1	0.0800	...
Medium	384	192	1.21×10^2	0.0642	1.84
High	576	288	1.35×10^2	0.0732	1.12
Highest	864	432	1.44×10^2	0.0711	1.06

sub-optimal energy (assuming white noise forcing). The number of grid points in the axial and radial directions is given by N_x and N_r, respectively, and these increase by a factor of 1.5 for each row. The final column lists the convergence factor defined as the ratio of the maximum gain to the maximum gain obtained on the previous, coarser mesh. For the higher mesh resolutions, we conclude that the results converge with respect to the mesh resolution. In this study, we have used the grid with high resolution.

TABLE II. Input and output domains and corresponding optimal singular values and sub-optimal energy percentages for the $M_j = 1.5$ supersonic jet for forcing frequency $St = 0.33$.

Label	x_{min}	x_{max}	r_{min}	r_{max}	σ_1	$\frac{\sum\sigma^2_{sub-optimal}}{\sum\sigma^2_{total}}$
I1	−10.0	60.0	0.29	2.90	1.35×10^2	0.0732
I2	−10.0	50.6	0.29	2.90	1.35×10^2	0.0669
I3	−10.0	30.2	0.29	2.90	1.35×10^2	0.0497
R1	−10.0	60.0	8.70	39.2	1.35×10^2	0.0732
R2	−10.0	50.6	8.70	39.2	1.15×10^2	0.0874
R3	−10.0	60.0	8.70	14.9	8.34×10^1	0.0544
R4	−10.0	50.6	8.70	14.9	8.09×10^1	0.0524
R5	−10.0	30.2	8.70	39.2	5.26×10^1	0.2181

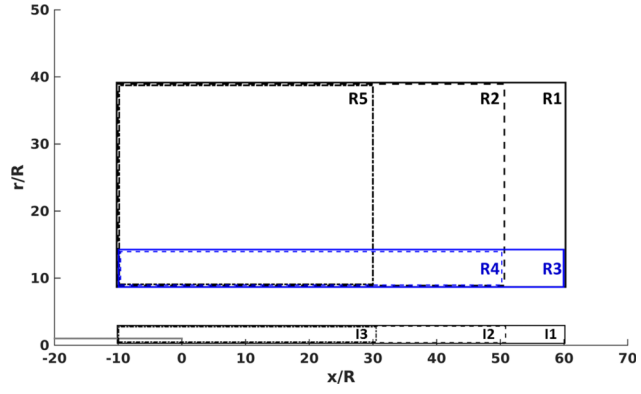

FIG. 20. Graphical representation of various input and output domains.

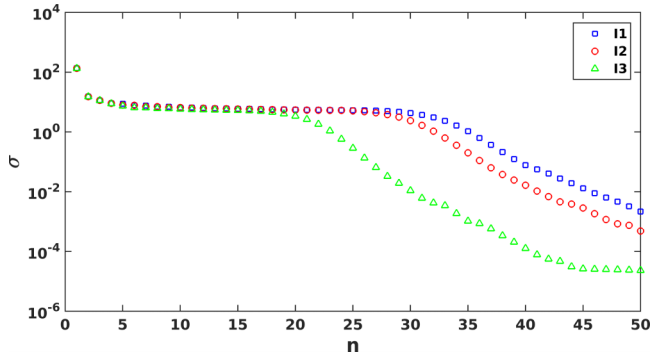

FIG. 21. Gains for various input domains for the $M_j = 1.5$ supersonic jet for forcing frequency $St = 0.33$.

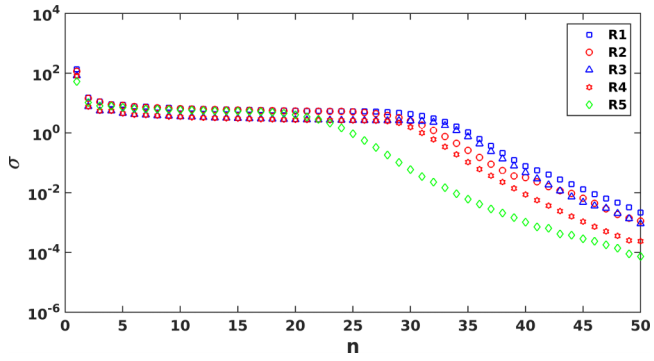

FIG. 22. Gains for various output domains for the $M_j = 1.5$ supersonic jet for forcing frequency $St = 0.33$.

B. Domain independence

To investigate the dependence of the gains on the input and output domain sizes, we consider five different output domains and three different input domains. These domains are summarized in Table II and displayed graphically in Fig. 20. The input domains (I1-I3) are restricted to the region close to the jet shear layer, whereas the output domains (R1-R5) are restricted to the far-field region. As mentioned in Sec. II, the input forcing is selected to choose velocity through the matrix B, while the matrix C selects pressure from the state vector. Specifically, the input and output domains defined in Sec. II and used throughout the study (unless otherwise stated) correspond here to I1 and R1, respectively. Physically, this choice was made to capture the influence of velocity fluctuations

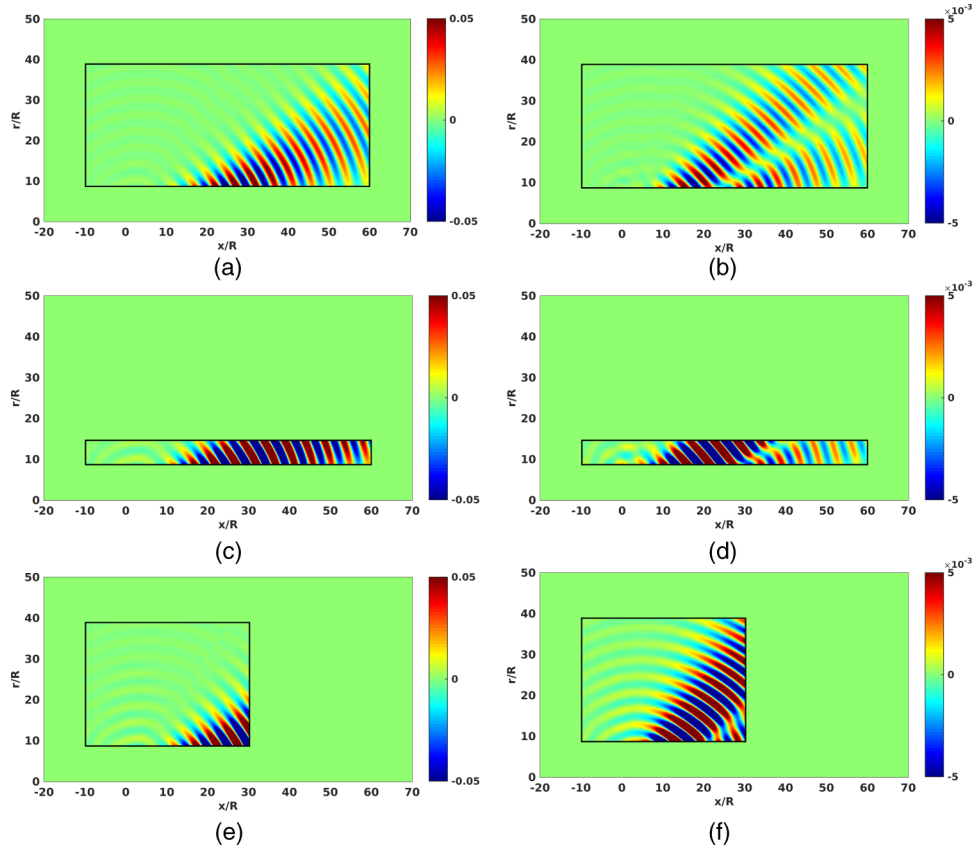

FIG. 23. The optimal and the first sub-optimal output modes of the $M_j = 1.5$ supersonic jet for forcing frequency $St = 0.33$ with the output domains (top) R1, (middle) R3, and (bottom) R5. (a,c,e) $n = 1$. (b,d,f) $n = 2$.

inside the full jet on the far-field pressure fluctuations. By systematically varying the input and output domain sizes, however, we assess the robustness of our results to this particular choice.

The three different input domains were tested using the same output domain R1. For the optimal mode, Fig. 21 shows that input-output analysis produces almost the same results regardless of the input domain sizes. Since the input mode shown in Fig. 3(a) fully resides inside all three input domains, this is not surprising. Because the sub-optimal modes extend farther downstream as mode number increases, the dropoff in singular values is affected by the length of the input domain.

The effect of the output domain size was examined in terms of the gains for the $M_j = 1.5$ jet. Each case used I1 as the input domain. As expected, output domains that extend farther in the lateral or the axial directions result in larger amplification than smaller domains. In Fig. 22, however, the gains for output domain having the same axial extent follow the same curve, shifted vertically by a relatively constant offset. Again, the dropoff in singular values at high mode numbers is determined by the axial length of the output domain. Furthermore, as Fig. 23 shows, the shape of the output modes remains unchanged in the areas where the output domains overlap. This means that the mode selected is not sensitive to the details of the chosen output domain. Rather, we observe the same physical mode through different windows.

V. CONCLUSIONS

The present study considers input-output analysis of small perturbations about RANS and LES base flows for subsonic and supersonic isothermal jets. The linearized Euler equations govern the dynamics of small perturbations about the base flows. Singular value decomposition of the resolvent operator yields orthonormal sets of corresponding input and output modes. For a given frequency, the leading output mode, associated with the largest singular value, recovers a convectively unstable wavepacket similar to that obtained by analysis of the PSE.

While the leading output mode represents the optimal linear response to forcing, input-output analysis also predicts a range of sub-optimal modes, associated with lesser singular values. These sub-optimal modes correspond to additional coherent forcings and responses. Moreover, the sub-optimal output modes follow a regular pattern, where acoustic radiation is organized into an increasing number of acoustic beams leaving the jet at different angles. As the mode number increases, output modes tend to include more acoustic beams oriented both towards the sideline direction and low angles with respect to the jet axis.

By repeating input-output analysis for 13 different base flows, we investigate the effect of jet Mach number on the importance of sub-optimal modes in the prediction of jet noise. For supersonic jets, the largest singular value is much greater in magnitude than any of the others, and thus, the acoustic response is dominated by the leading output mode. Additionally, the leading input mode in this case is confined inside the nozzle and in the immediate vicinity of its exit. Physically, this agrees with an instability wave mechanism triggered by a small upstream disturbance, and analysis of the PSE successfully predicts the acoustic response in this case. For subsonic jets, however, the gains corresponding to sub-optimal modes are comparable to the amplification of the leading mode and therefore cannot be neglected.

This parametric study also suggests the importance of a new dimensionless parameter, the acoustic Strouhal number St_a defined in terms of the free-stream speed of sound. We show that the acoustic Strouhal number determines the number of significant sub-optimal modes regardless of the jet Mach number. By retaining only the optimal mode and the significant sub-optimal modes, we may construct an accurate but minimal reduced-order model of noise generation at a given frequency.

We further assess the relevance of sub-optimal modes by projecting data obtained from an LES of a supersonic jet onto the orthonormal sets of singular directions resulting from input-output analysis. Projection onto input modes determines the relative amplitude of each mode, as forced by the jet turbulence. We find that sub-optimal modes are quite active, even in this case which is otherwise dominated by the optimal mode. In fact, taking into account sub-optimal modes with projected amplitudes increases the output sound pressure level by 0.37 dB for this jet. The LES data

projection onto the output modes confirms their physical relevance and further demonstrates the potential of input-output analysis for reduced-order modeling of jet noise. With only 24 modes, we find that input-output analysis recovers a substantial amount of the acoustic energy predicted by the LES.

In the literature, it has been suggested that turbulent mixing noise is best represented by a two source model.[44,45] In particular, experimental measurements seem to fit two independent mechanisms of jet noise generation. In this view, one mechanism is associated with large scale coherent structures and is responsible for downstream acoustic radiation known as the large scale spectrum (LSS). The other mechanism is thought to be more incoherent and omnidirectional in nature and creates the fine scale spectrum (FSS). As recently argued, however, it may be possible to model jet noise with a single source model which does not separate between LSS and FSS.[16,46] Our results further suggest that sideline radiation can be explained by coherent mechanisms associated with sub-optimal modes, in addition to the downstream radiation associated with the optimal mode. Based on the LES data projection onto the set of output modes, we find that including sub-optimal modes results in a 10–20 dB increase in far-field SPL for polar angles $\phi > 40°$.

We have limited the scope of the present study to axisymmetric isothermal high-speed jets. In future work, cold and hot jets will be adopted as base flows. Also, work is underway to investigate higher azimuthal wavenumber modes such as $m = 1$ (helical) and $m = 2$ in addition to the axisymmetric modes ($m = 0$). We also suggest that the flexibility of input-output analysis through the choice of the B and C matrices could be exploited to understand which source terms or combinations of source terms produce most noise. This could be repeated for different formulations of the LEE to determine whether any are superior. Finally, while we have analyzed a high-fidelity LES database for a supersonic jet, a similar analysis should be applied to a subsonic jet to further investigate the relevance of sub-optimal modes.

ACKNOWLEDGMENTS

This research was supported in part by the Aerospace Engineering and Mechanics Department's faculty startup fund at the University of Minnesota, the University of Minnesota Informatics Institute Transdisciplinary Faculty Fellowship, and the National Science Foundation under Award No. CMMI 1363266. J.W.N. and M.R.J. gratefully acknowledge support during the 2014 Summer Program at the Center for Turbulence Research at Stanford University where this work was initiated. Discussions with S. Lele, T. Colonius, P. Jordan, P. Schmid, and M. Juniper are gratefully acknowledged. High-fidelity simulations were enabled by grants of computer time at the ERDC and AFRL supercomputing centers as well as at the Argonne National Laboratory.

[1] M. Lighthill, "On sound generated aerodynamically. I. General theory," Proc. R. Soc. A **211**, 564–587 (1952).
[2] N. Curle, "The influence of solid boundaries upon aerodynamic sound," Proc. R. Soc. A **231**, 505–514 (1955).
[3] J. Ffowcs Williams, "The noise from turbulence convected at high speed," Philos. Trans. R. Soc., A **255**, 469–503 (1963).
[4] G. Lilley, "On the noise from jets," in *AGARD-CP-131* (Advisory Group for Aeronautical Research and Development, 1974).
[5] M. Goldstein, "A generalized acoustic analogy," J. Fluid Mech. **488**, 315–333 (2003).
[6] M. Goldstein and S. Leib, "The aeroacoustics of slowly diverging supersonic jets," J. Fluid Mech. **600**, 291–337 (2008).
[7] S. Karabasov, M. Afsar, T. Hynes, A. Dowling, W. McMullan, C. Pokora, G. Page, and J. McGuirk, "Jet noise: Acoustic analogy informed by large eddy simulation," AIAA J. **48**, 1312–1325 (2010).
[8] E. Mollo-Christensen, "Measurements of near field pressures of subsonic jets," Tech. Rep. ASRL TR 1009, Massachusetts Institute of Technology, Aeroelastic and Structures Research Laboratory, Cambridge, MA, April 1963.
[9] E. Mollo-Christensen, "Jet noise and shear flow instability seen from an experimenter's viewpoint," J. Appl. Mech. **34**, 1–7 (1967).
[10] T. Suzuki and T. Colonius, "Instability waves in a subsonic round jet detected using a near-field phased microphone array," J. Fluid Mech. **565**, 197–226 (2006).
[11] J. B. Freund, "Noise sources in a low-Reynolds-number turbulent jet at Mach 0.9," J. Fluid Mech. **438**, 277–305 (2001).
[12] L. C. Cheung, D. J. Bodony, and S. K. Lele, "Noise radiation predictions from jet instability waves using a hybrid nonlinear PSE-acoustic analogy approach," AIAA Paper 2007-3638, 2007.
[13] K. Gudmundsson and T. Colonius, "Instability wave models for the near-field fluctuations of turbulent jets," J. Fluid Mech. **689**, 97–128 (2011).
[14] D. Rodríguez, A. Sinha, G. A. Brès, and T. Colonius, "Inlet conditions for wave packet models in turbulent jets based on eigenmode decomposition of large eddy simulation data," Phys. Fluids **25**, 105107 (2013).

[15] A. Sinha, D. Rodríguez, G. A. Brès, and T. Colonius, "Wavepacket models for supersonic jet noise," J. Fluid Mech. **742**, 71–95 (2014).
[16] P. Jordan and T. Colonius, "Wave packets and turbulent jet noise," Annu. Rev. Fluid Mech. **45**, 173–195 (2013).
[17] A. Towne and T. Colonius, "Improved parabolization of the Euler equations," AIAA Paper 2013-2171, 2013.
[18] J. W. Nichols and S. K. Lele, "Global modes and transient response of a cold supersonic jet," J. Fluid Mech. **669**, 225–241 (2011).
[19] A. V. Cavalieri, P. Jordan, A. Agarwal, and Y. Gervais, "Jittering wave-packet models for subsonic jet noise," J. Sound Vib. **330**, 4474–4492 (2011).
[20] P. Jordan, T. Colonius, G. Brés, M. Zhang, A. Towne, and S. Lele, "Modeling intermittent wavepackets and their radiated sound in a turbulent jet," in *Proceedings of the Summer Program* (Center for Turbulence Research, Stanford University, 2014), pp. 241–249.
[21] C. K. Tam and F. Q. Hu, "On the three families of instability waves of high-speed jets," J. Fluid Mech. **201**, 447–483 (1989).
[22] X. Garnaud, L. Lesshafft, P. Schmid, and P. Huerre, "The preferred mode of incompressible jets: Linear frequency response analysis," J. Fluid Mech. **716**, 189–202 (2013).
[23] L. Trefethen, A. Trefethen, S. Reddy, T. Driscoll *et al.*, "Hydrodynamic stability without eigenvalues," Science **261**, 578–584 (1993).
[24] A. Monokrousos, E. Åkervik, L. Brandt, and D. S. Henningson, "Global three-dimensional optimal disturbances in the Blasius boundary-layer flow using time-steppers," J. Fluid Mech. **650**, 181–214 (2010).
[25] D. Sipp and O. Marquet, "Characterization of noise amplifiers with global singular modes: The case of the leading-edge flat-plate boundary layer," Theor. Comput. Fluid Dyn. **27**, 617–635 (2013).
[26] P. J. Schmid and D. S. Henningson, *Stability and Transition in Shear Flows*, Applied Mathematical Sciences Vol. 142 (Springer, 2001).
[27] M. R. Jovanović and B. Bamieh, "Componentwise energy amplification in channel flows," J. Fluid Mech. **534**, 145–183 (2005).
[28] J. W. Nichols and M. R. Jovanović, "Input-output analysis of high-speed jet noise," in *Proceedings of the Summer Program* (Center for Turbulence Research, Stanford University, 2014), pp. 251–260.
[29] R. Moarref, M. Jovanović, J. Tropp, A. Sharma, and B. McKeon, "A low-order decomposition of turbulent channel flow via resolvent analysis and convex optimization," Phys. Fluids **26**, 051701-1–051701-7 (2014).
[30] A. T. Thies and C. K. Tam, "Computation of turbulent axisymmetric and nonaxisymmetric jet flows using the k-ε model," AIAA J. **34**, 309–316 (1996).
[31] G. A. Brès, J. W. Nichols, S. K. Lele, and F. E. Ham, "Towards best practices for jet noise predictions with unstructured large eddy simulations," AIAA Paper 2012-2965, 2012.
[32] J. W. Nichols, S. Lele, and P. Moin, "Global mode decomposition of supersonic jet noise," in *Annual Research Briefs* (Center for Turbulence Research, Stanford University, 2009).
[33] A. Jameson, "Aerodynamic design via control theory," J. Sci. Comput. **3**, 233–260 (1988).
[34] A. Jameson, "Re-engineering the design process through computation," J. Aircr. **36**, 36–50 (1999).
[35] J. C. Newman III, A. C. Taylor III, R. W. Barnwell, P. A. Newman, and G. J.-W. Hou, "Overview of sensitivity analysis and shape optimization for complex aerodynamic configurations," J. Aircr. **36**, 87–96 (1999).
[36] G. J. Chandler, M. P. Juniper, J. W. Nichols, and P. J. Schmid, "Adjoint algorithms for the Navier-Stokes equations in the low Mach number limit," J. Comput. Phys. **231**, 1900–1916 (2012).
[37] S. Leib and M. Goldstein, "Hybrid source model for predicting high-speed jet noise," AIAA J. **49**, 1324–1335 (2011).
[38] Y. Khalighi, A. Mani, F. Ham, and P. Moin, "Prediction of sound generated by complex flows at low Mach numbers," AIAA J. **48**, 306–316 (2010).
[39] A. Mani, "Analysis and optimization of numerical sponge layers as a nonreflective boundary treatment," J. Comput. Phys. **231**, 704–716 (2012).
[40] R. B. Lehoucq, D. C. Sorensen, and C. Yang, *Users' Guide: Solution of Large-Scale Eigenvalue Problems with Implicitly Restarted Arnoldi Methods* (SIAM, 1998).
[41] C. K. Tam, "Supersonic jet noise," Annu. Rev. Fluid Mech. **27**, 17–43 (1995).
[42] A. P. Dowling and J. Ffowcs Williams, *Sound and Sources of Sound* (Horwood, 1983).
[43] X. Garnaud, R. D. Sandberg, and L. Lesshafft, "Global response to forcing in a subsonic jet: Instability wavepackets and acoustic radiation," AIAA Paper 2013-2232, 2013.
[44] C. K. Tam, M. Golebiowski, and J. M. Seiner, "On the two components of turbulent mixing noise from supersonic jets," AIAA Paper No. 96-1716, 1996.
[45] C. K. Tam, K. Viswanathan, K. Ahuja, and J. Panda, "The sources of jet noise: Experimental evidence," J. Fluid Mech. **615**, 253–292 (2008).
[46] D. Papamoschou, "Wavepacket modeling of the jet noise source," AIAA Paper 2011-2835, 2011.